HHS Public Access

Author manuscript

Nat Cell Biol. Author manuscript; available in PMC 2015 November 01.

Published in final edited form as:

Nat Cell Biol. 2015 May ; 17(5): 558–568. doi:10.1038/ncb3143.

Independent and coordinate trafficking of single *Drosophila* germ plasm mRNAs

Shawn C. Little[1,2], **Kristina S. Sinsimer**[1], **Jack J. Lee**[1], **Eric F. Wieschaus**[1,2], and **Elizabeth R. Gavis**[1,3]

[1]Department of Molecular Biology, Princeton University, Princeton, NJ 08544

[2]Howard Hughes Medical Institute, Princeton University, Princeton, NJ 08544

Abstract

mRNA localization is a conserved mechanism for spatial control of protein synthesis, with key roles in generating cellular and developmental asymmetry. While different transcripts may be targeted to the same subcellular domain, the extent to which their localization is coordinated is unclear. Using quantitative single molecule imaging, we analyzed the assembly of *Drosophila* germ plasm mRNA granules inherited by nascent germ cells. We find that the germ cell-destined transcripts *nanos*, *cyclin B*, and *polar granule component* travel within the oocyte as ribonucleoprotein particles containing single mRNA molecules but co-assemble into multi-copy heterogeneous granules selectively at the posterior of the oocyte. The stoichiometry and dynamics of assembly indicate a defined stepwise sequence. Our data suggest that co-packaging of these transcripts ensures their effective segregation to germ cells. In contrast, compartmentalization of the germline determinant *oskar* mRNA into different granules limits its entry into germ cells. This exclusion is required for proper germline development.

INTRODUCTION

Intracellular localization of mRNAs is a widespread strategy for targeting the encoded proteins to regions of the cell where they function. mRNAs travel as ribonucleoprotein particles (RNPs), whose associated proteins direct their localization through interactions with molecular motors, cytoskeletal elements, and/or other cellular components[1,2]. These RNPs can contain many mRNAs, several mRNAs, or only a single mRNA molecule, depending on the cell type, context, and possibly the mechanism of localization[3–8]. How RNP composition is determined, how multiple mRNAs are co-assembled into RNPs, and where assembly occurs remain poorly understood.

The *Drosophila* germ plasm, whose assembly and function rely on localized mRNAs, provides an ideal system to address these questions. This specialized cytoplasm at the

[3]Corresponding author (gavis@princeton.edu).

AUTHOR CONTRIBUTIONS

S.C.L, K.S.S., and E.R.G. designed the experiments. S.C.L, K.S.S., J.J.L. and E.R.G. performed the experiments. S.C.L. and E.R.G. analyzed the data. S.C.L., E.R.G., and E.F.W. wrote the manuscript.

posterior of the embryo is necessary and sufficient for induction of the germ cell progenitors, the pole cells[9]. Numerous maternal mRNAs are enriched within the germ plasm and then inherited by the pole cells[10,11], where they direct production of proteins required for specification of germline fate and for germline development[12,13]. Formation of the germ plasm is initiated during mid-oogenesis by the kinesin-dependent transport of *oskar* (*osk*) mRNA to the posterior of the oocyte. Osk protein produced from this localized RNA recruits the helicase Vasa (Vas) and other proteins, establishing a posterior domain of germ plasm assembly[14]. This initial step is essential for a second wave of mRNA localization during late stages of oogenesis, whereby additional *osk* as well as numerous other mRNAs including *nanos* (*nos*), *polar granule component* (*pgc*), and *cyclin B* (*cycB*) accumulate at the posterior[15–18]. Live imaging of *nos* mRNA showed that its localization occurs as a consequence of diffusion within the oocyte cytoplasm and entrapment at the posterior in Vas-containing RNPs known as polar granules[16]. Later, during embryogenesis, these granules are segregated to the pole cells as those cells bud from the posterior of the embryo[19].

The accumulation of numerous different mRNAs within the germ plasm via a common localization pathway and their ultimate destination in the pole cells begs the question of whether their trafficking is coordinated at any step. Moreover, whether the movement of multiple mRNAs to the posterior pole and ultimately into the pole cells is coordinated through co-packaging into common RNPs or whether they are organized into functionally distinct RNPs has not been investigated. To address these questions, we analyzed the mRNA composition of RNPs containing germ plasm mRNAs at different stages of oogenesis and embryogenesis by high resolution fluorescent in situ hybridization (FISH) and quantitative image analysis. Using *nos* as a paradigm, we show that localization occurs by the exclusive assembly of RNPs containing single mRNAs into multi-copy granules at the posterior cortex. Co-packaging of *nos* with *cycB* and *pgc* occurs selectively at the posterior, forming heterogeneous polar granules that co-transport germ plasm mRNAs into pole cells. In contrast, *osk* travels in multi-copy RNPs and is segregated from the other mRNAs at the posterior into compositionally distinct granules that can contain hundreds of *osk* transcripts. These granules must be excluded from the pole cells for germline development.

RESULTS

nos mRNAs travel as single-copy particles prior to posterior localization

To better understand how *nos* becomes assembled into polar granules, we performed fluorescence in situ hybridization (FISH) using a method capable of detecting individual mRNA molecules in *Drosophila* embryos[20,21] (Supplementary Video 1). We observed two classes of labeled objects: dim punctae at high density filling the embryo interior and bright objects near the cortical surface at the posterior (Fig. 1a,b). Both classes appear as diffraction-limited point sources (Supplementary Fig. 1a). Visualized in sections near the mid-sagittal plane, the bright objects occupy a cap-shaped volume covering the posterior at a depth up to ~5 μm beneath the cortex (Fig. 1b). The posterior cap extends ~25 μm from the posterior pole, measured as an arc along the cortical surface (Fig. 1a). Localization of *nos* is observed as an increase in fluorescent signal close to posterior pole, resulting from the

enrichment of bright objects containing many mRNAs (i.e., localized granules) accompanied by a depletion of dim punctae (i.e., unlocalized particles) that contain fewer mRNAs (Supplementary Fig. 1b–d).

We quantified the mRNA content of the unlocalized particles by comparing the number of particles detected by FISH to the number of mRNAs measured by absolute RT-qPCR. Counting dim punctae in the entire left or right halves of embryos and multiplying by two yields an estimate of $2.0 \pm 0.5 \times 10^6$ objects per embryo. Our ability to detect most dim objects was confirmed by FISH using *nos* probes alternating in fluorophore color along the length of the transcript. Plotting the distribution of fluorescence intensities for detected objects in each channel in two-dimensional (2D) histograms, we found that ≥97% of dim objects detected in one channel also appear in the second channel (Fig. 1c,d), indicating high detection efficiency. The total number of detected particles in the embryo ($2.0 \pm 0.5 \times 10^6$) approximates the total number of *nos* mRNA molecules per embryo determined by RT-qPCR ($2.5 \pm 0.4 \times 10^6$, Supplementary Fig. 1e). Thus, the average mRNA content of the imaged dim punctae is 1.3 ± 0.5 mRNAs. Since only ~4% of *nos* mRNA is localized[22] (also see Methods), unlocalized particles, which constitute the vast majority of *nos* mRNA in embryos, largely represent single mRNAs.

Given the high density of unlocalized *nos* particles, we estimate that ~15% of unlocalized transcripts reside within the same imaging volume by random chance (Supplementary Fig. 1f–j and Methods). Co-localization detected in excess of this amount would thus indicate concerted co-packaging of multiple *nos* mRNAs. To estimate the fraction of unlocalized particles containing >1 *nos* transcript, we examined the fluorescence intensity distributions in 2D histograms after normalizing to the most frequently observed intensity in each channel. Because the number of probes decorating each mRNA molecule is drawn at random from a distribution about the mean number of probes, the two intensity measurements should be uncorrelated for particles representing single mRNAs. We observed a weak correlation with a clear skew toward higher mRNA content along the correlated axis (Fig. 1e,f, cyan) compared with the symmetric distribution along the anticorrelated axis (Fig. 1e,f, red). The distribution along the correlated axis is well matched by model in which 83% and 15% of detected punctae represent 1 and 2 mRNAs, respectively (Fig. 1f). Thus, the predicted rate of spurious co-localization within the same volume is similar to the observed frequency of punctae containing 2 mRNAs. We conclude that unlocalized *nos* exists as single mRNAs that are not co-packaged prior to localization.

nos localization results from the spatially restricted assembly of multi-copy granules

In two-color FISH experiments, normalized intensity values for each fluorophore in granules at the posterior pole are highly correlated, indicating that in contrast to unlocalized *nos* particles, these granules contain multiple *nos* transcripts (Supplementary Fig. 1k). Normalization to the intensity of single molecules observed in the dim punctae permits estimation of granule size in absolute mRNA numbers. Posterior cortical localization of *nos* results from the enrichment of granules containing >4 *nos* mRNAs (Fig. 1g,h, Supplementary Fig. 1k,l) that, as expected, do not form in *osk* or *vas* mutant embryos (Supplementary Fig. 1m,n). *nos* content of individual granules spans a wide range and can

be >60 transcripts, with a mean of 16 (Fig. 1g,h). The variability in mRNA content (standard deviation = 12) is on the same order as the mean, indicating significant heterogeneity in mRNA content among localized granules (Supplementary Fig. 1o). A Poisson process that produces a mean of 16 mRNAs per granule by random arrival at sites of granule formation would predict a standard deviation of only four mRNAs. In support of a more complicated granule assembly process, we observed that localized *nos* content in these granules is not normally distributed and is better described by a log-normal fit characteristic of an exponential growth process in which growth rate scales with granule size (Fig. 1g; see Discussion).

The localization of *nos* occurs during late stages of oogenesis. To determine when and where the transition from single mRNAs to multi-copy granules occurs and the relationship between granule formation and posterior localization, we analyzed *nos* during this period (Fig. 2a). Synthesized by the ovarian nurse cells, *nos* enters the oocyte en masse when the nurse cells "dump" their contents at the end of stage 10 and becomes distributed throughout the oocyte by diffusion and the concurrent streaming of the oocyte cytoplasm (ooplasm)[16]. Consistent with previous analysis of *nos* mRNA labeled using the MS2/MS2 coat protein (MCP) system[16], we observed continuous accumulation of *nos* in granules at the posterior of the oocyte beginning at stage 10 of oogenesis. *nos*-containing granules increase in both number and mRNA content up until the oocyte reaches maturity at stage 14 (Fig. 2b). Similarly to the early embryo, multi-copy granules were observed only within a depth of ~5 μm from the cortex and only within the localization domain (Supplementary Fig. 2a).

The appearance of localized granules as diffraction-limited objects (Supplementary Fig. 1a) suggests that they correspond to individual higher order RNPs containing many mRNAs. To support the idea that the bright objects represent physically associated mRNA particles and not particles transiently corralled into the same volume, we compared our FISH data to data from live imaging of MS2-tagged *nos* labeled with MCP-GFP (*nos**GFP). Localized *nos**GFP granules have a spatial distribution and fluorescence intensities similar to those of *nos* granules detected by FISH, indicating that they likely represent the same entities (Fig. 2d). Previous live imaging experiments showed that *nos**GFP granules undergo rapid, directed movement along microtubules at the posterior cortex.[23] By performing a chi square fit to match to the right sides of the fluorescence intensity distributions of *nos* granules detected by FISH and *nos**GFP granules in live oocytes, we found that objects undergoing rapid, directed runs over several micrometers at ≥0.5 μm/s contain upwards of 10–20 *nos* mRNAs (Fig. 2d). Throughout each run, the intensity measurement remains unchanged, indicating that the detected mRNAs are constituents of the same granule (Fig. 2e, Supplementary Fig. 2b–d, Supplementary Video 2). Taken together, our results indicate that *nos* localization results from the incorporation of single transcript particles into multi-copy granules exclusively at the posterior cortex.

Germ plasm mRNAs assemble into common but heterogeneous granules at the posterior

Because numerous mRNAs in addition to *nos* are localized to the germ plasm and incorporated into pole cells[10,11], we hypothesized that their localization might be coordinated through co-packaging into the same RNPs. To determine if and when co-

packaging occurs, we examined the distributions of two additional germ plasm mRNAs, *pgc* and *cycB*, in pairwise combinations with *nos*. All three mRNAs are expressed at high levels in the nurse cells at mid-oogenesis (Fig. 3a–d). Around stage 10, prior to the onset of nurse cell dumping, they become enriched on colecemid-sensitive track-like structures, likely microtubules, that are best visualized at the cortical surface (Fig. 3c). Tracks are also detected that extend toward the ring canal junctions connecting nurse cells to the oocyte and to each other (Fig. 3d). Despite their similar distributions, we did not detect co-localization of *nos*, *pgc*, or *cycB* mRNAs prior to posterior localization, in either the nurse cells or bulk ooplasm (Supplementary Fig. 3a–d).

Once they reach the posterior, *pgc* and *cycB* mRNAs, like *nos*, begin to form large granules (Fig. 3e–j). To determine whether *nos* and *pgc* can reside within the same polar granule, we calculated the distance in 3D space between nearest neighbors in the two channels. In the 2-color *nos* FISH experiments described above, >95% of localized granules detected in one channel possessed a partner in the other channel at a distance of <200 nm (<3 pixels in the xy plane). Given a density of about 0.7 granules/μm^3, the expected co-localization rate due to random chance is ~10% (see Methods). Using 200 nm as the criterion for co-localization, we found that by late oogenesis 33% of *nos* granules contain *pgc*, and conversely 62% of localized *pgc* contains *nos* (Fig. 3j). The frequent overlap of *pgc* and *nos* granules suggests that *nos* and *pgc* mRNAs are physically linked. Similar results were obtained for *nos* and *cycB* (Supplementary Fig. 3e,f). We conclude that different germ plasm mRNAs co-assemble in granules exclusively at the posterior cortex.

Dual mRNA labeling experiments showed that a substantial fraction of localized granules contain only one of two different mRNAs regardless of the copy number of that mRNA (Fig. 3h–j, Supplementary Fig. 3f). In contrast, the vast majority of granules containing >5 molecules of *nos* or *cycB* either alone or combined together exhibit co-localization with granules of Vas, visualized by direct fluorescence of GFP-Vas (Fig. 4). The co-localization of germ plasm mRNAs with GFP-Vas occurs in the same spatial domain where we observe their enrichment, consistent with a model wherein Vas activity at the posterior is required to recruit single-copy mRNA particles into nascent granules. Moreover, a small fraction (6%) of localized GFP-Vas objects lack both *nos* and *cycB* (Fig. 4j) but likely contain other posteriorly localized mRNAs. The enrichment of granules completely lacking any given mRNA rules out a simple model of granule assembly by random selection of mRNAs from the unlocalized pool. Such a model predicts that, for granules of a given total size, the fraction containing at least one transcript from a particular gene must always be greater than the fraction containing zero copies of that mRNA (Supplementary Fig. 4). This is not observed in the dual mRNA labeling experiments, where the fraction containing zero copies is notably enriched (Fig. 3c, Supplementary Figs. 3f and 4). Instead, our data are consistent with a model in which 1) transcripts of a given gene are preferentially incorporated into granules through the formation of homotypic mRNA clusters, and 2) homotypic clusters containing different mRNAs associate in higher-order assemblies to form heterogeneous polar granules.

osk multimerization in the nurse cells and anterior oocyte precedes assembly of large localized granules

In contrast to other germ plasm mRNAs, posterior localization of *osk* occurs in two mechanistically distinct phases. During mid-oogenesis, *osk* is transported to the posterior in RNPs containing the double-stranded RNA binding protein Staufen (Stau), which may link *osk* to kinesin and is required for *osk* translational activation and anchoring at the posterior cortex[24–26]. In addition, *osk* mRNA forms higher order complexes that may play a role in repression of *osk* translation and coordination of *osk* transport[8,27,28]. The *osk* mRNA content of these complexes, and where and when they form, has not been determined. During late oogenesis, *osk* is localized along with other germ plasm mRNAs by diffusion and posterior entrapment[15,29]. We investigated the nature of *osk* RNP complexes during both phases of localization using methods described above for *nos* to confirm detection of single *osk* mRNAs (Supplementary Fig. 5a–d) and correspondence between objects observed in live and fixed oocytes (Supplementary Fig. 5e–h).

Like *nos*, *cycB*, and *pgc*, *osk* is highly expressed in nurse cells and can be found on track-like structures during mid-oogenesis (Supplementary Fig. 5i). However, *osk* exhibits several differences from *nos*. First, whereas *nos* is found uniformly in all nurse cells as single mRNAs, a large fraction of *osk* particles in nurse cells contain two mRNAs at levels that are twice as high as expected from random co-localization alone (Fig. 5 and Methods). Second, among nurse cells at the posterior of the cluster, the nurse cell connected exclusively to the oocyte and to no other nurse cells contains less *osk* overall, as well as a lower ratio of particles containing two *osk* mRNAs compared to other nurse cells (0.8 versus 0.4 particles/μm^3; Fig. 5, Fig. 6b,c). These observations are explained by a mathematical model in which 2-copy particles are preferentially transported between nurse cells as well as between nurse cells and oocyte (Supplementary Note), suggesting that the formation of 2-copy particles enhances *osk* transport to the oocyte. Third, *osk* particles containing 2–4 mRNAs are heavily enriched in the ooplasm from mid-oogenesis onward and persist in the bulk cytoplasm of the early embryo. Colocalization of *osk* with Stau-GFP was first detected in the oocyte, coinciding with the formation of *osk* particles containing > 2 mRNAs at the anterior and persisting in localized granules (Fig. 5). These results show that, unlike *nos* and other germ plasm mRNAs, posterior localization of *osk* is preceded by the assembly in the oocyte of RNPs containing Stau and multiple *osk* mRNAs.

We next examined the posterior cortical enrichment of *osk* once it enters the oocyte. We observed bright granules at the posterior cortex during stages 8 and 9 of oogenesis, but the high density of *osk* in the ooplasm through stage 8 (Fig. 6a–d) precluded us from determining if these granules assemble prior to their arrival at the posterior. By stage 9, *osk* in the bulk ooplasm is found in 1- to 4-copy punctae, with nearly all brighter granules near the posterior cortex (Fig. 6e–g), where they grow in both number and mRNA content through the end of oogenesis (stage 14). Like *nos*, the distribution of *osk* mRNA content in localized granules is heterogeneous and can be described by a log-normal distribution (Supplementary Fig. 5j,k). Total *osk* content per granule approaches a maximum of ~250 mRNAs during late oogenesis (Fig. 6h). From stage 10 onward, a large majority (>90%) of granules containing 50 or more *osk* mRNAs are found ≤5 μm beneath the cortex, within 30

μm of the posterior pole as measured along the surface of the cortex (Fig. 6i). Thus, large *osk* granules reside within the same domain where *nos* granules subsequently form. Particles containing small numbers (2–4) of *osk* mRNAs are depleted at the posterior cortex (Fig. 6j), suggesting that the large localized granules are assembled preferentially from the smaller *osk* RNPs. These results indicate that localization occurs through *osk* granule assembly in a unique manner distinct from other posteriorly localized mRNAs, with the formation of particles containing 2 *osk* mRNA molecules in nurse cells, the association of these upon entry to the oocyte to form particles containing 4 *osk* transcripts and, by late oogenesis, the assembly of large complexes that contain hundreds of mRNAs.

osk mRNA is continuously segregated from germ granules

The accumulation of *osk* at the posterior cortex in multi-copy granules concomitantly with *nos* and other germ plasm mRNAs during late oogenesis raised the possibility that *osk* might be incorporated into the same localized granules. We therefore performed dual FISH for *nos* and *osk* in oocytes with expressing either GFP-Vas or Osk-GFP. Granules of localized *osk* mRNA inhabit regions devoid of *nos*, GFP-Vas or Osk-GFP (Fig. 7a–j). Nearest neighbor distance measurements confirmed that 90% of particles containing *nos* mRNA co-localize with GFP-Vas or Osk-GFP. In contrast, <25% of the detected *osk* mRNA granules reside within 200 nm of a granule containing *nos*, GFP-Vas, and/or Osk-GFP (Fig. 7k). Rather, localized *osk* granules show 90% concordance with Stau-GFP (Fig. 5c), suggesting a role for Stau in the late localization of *osk* in addition to its earlier role in *osk* transport. These results indicate that *osk* mRNA is segregated from *nos* and other germ plasm RNAs by incorporation into compositionally distinct granules.

Localization of *osk* to germ granules impairs germ cell formation

The segregation of *osk* from *nos* is maintained into embryogenesis (Fig. 8a). Prior to pole cell formation, *nos* granules dissociate from the cortex and accumulate around the centrosomes of posterior nuclei through dynein-dependent transport on astral microtubules. This trafficking promotes incorporation of *nos* along with the nuclei into pole cells as they bud from posterior of the embryo[19] (Fig. 8b,c). These granules retain other germ plasm mRNAs, as evidenced by the continued co-localization with *cycB* (Fig. 8d). Localized *osk* granules also dissociate from the cortex, but do not accumulate around posterior nuclei or become enriched in pole cells (Fig. 8b). By the onset of cellularization, *osk* granules are nearly absent from the posterior (Fig. 8c), whereas *nos* and other germ plasm mRNAs are highly enriched in pole cells (Fig. 8c–f; refs. [10,11]).

To determine whether *osk* is actively excluded from pole cells, we analyzed *osk-bcd3′UTR* embryos in which *osk* is mislocalized to the anterior by replacement of the *osk* 3′ untranslated region (3′UTR) with the *bicoid* (*bcd*) 3′UTR mRNA localization signal[30]. Osk protein produced at the anterior of *osk-bcd3′UTR* embryos results in ectopic germ plasm assembly and the induction of functional pole cells at the anterior[30]. Prior to this ectopic pole cell formation, a large fraction of granules at the anterior cortex contain both *osk* and *bcd* mRNAs (Fig. 8g). During pole cell formation, we unexpectedly observed the recruitment of granules containing exclusively *bcd* into regions surrounding prospective anterior pole cell nuclei whereas *osk*-containing granules are clearly excluded from the same

region (Fig. 8h). By the end of the blastoderm stage only *bcd* is highly enriched in ectopic pole cells even though large *osk* granules persist at the anterior beyond the time when endogenous *osk* at the posterior has largely disappeared (Fig. 8i). These results indicate that *osk* is effectively excluded from germ plasm granules that are segregated to the developing germline.

To determine the functional relevance of this exclusion, we examined the consequence of forcing *osk* localization to *nos*-containing polar granules. We generated an *osk* transgene that lacks features required for *osk* localization[31] and whose 3′UTR is substituted by the *nos* 3′UTR, which directs posterior localization and incorporation into pole cells[32] (*UAS-oskΔi1,2-nos3′UTR*). *oskΔi1,2-nos*3′UTR mRNA is highly co-localized with *nos* in polar granules, resulting in the segregation of *osk* mRNA to pole cells (Fig. 8j,k). Strikingly, both the amount of Vas in the pole cells and pole cell number are significantly reduced in *oskΔi1,2-nos*3′UTR embryos compared to control embryos (Fig. 8l). In contrast, no defects were observed in embryos expressing *gfp-nos3′UTR* mRNA, which was similarly localized to polar granules and incorporated into pole cells (Supplementary Fig. 6). Moreover, gonads of *oskΔi1,2-nos*3′UTR embryos contain few germ cells (Fig. 8m,n). This decrease is not due simply to overexpression of Osk protein, since embryos bearing 6 copies of a wild-type *osk* transgene develop an excess of pole cells[33]. These results indicate, therefore, that the inclusion of *osk* in germ plasm granules destined for pole cells is detrimental to pole cell induction and germline development.

DISCUSSION

Our quantitative analysis of germ plasm localized mRNAs has revealed several intriguing features about the localization process and the coordinate regulation of their integration into the pole cells. We show that *nos*, *pgc*, and *cycB* mRNAs are transported within the oocyte as single mRNAs and are co-packaged into granules specifically at the posterior cortex concomitant with localization. Thus, localization serves not only to concentrate these transcripts at the posterior, but generates large, multi-copy polar granules to coordinate the efficient incorporation of these transcripts into the pole cells.

Polar granules are heterogeneous with respect to both the amount of a particular mRNA and the combination of different mRNAs. While *nos* mRNA content of polar granules varies over a large range, there is a tendency toward higher values fitting a log-normal distribution. Log-normal distributions are often associated with exponential growth processes, whereby the rate at which an object grows is proportional to the size of the object[34,35]. Thus, a log-normal distribution suggests that large granules grow at faster rates compared to small ones as assembly is accelerated through positive feedback. Additionally, we find that for granules containing both *nos* and *pgc* or *nos* and *cycB*, the quantities of the two different mRNAs are somewhat correlated and there is a greater fraction of granules completely lacking one species of mRNA entirely than granules containing just a few copies of that mRNA. Together, these data suggest that for each type of mRNA, cooperative interactions generate homotypic RNPs that then 1) accelerate the recruitment of additional mRNAs of the same type, and 2) facilitate granule assembly by promoting interactions with similarly sized homotypic clusters of other mRNAs. These results also predict the existence of dedicated

molecular pathways, one to form homotypic clusters, and another to assemble homotypic clusters of many different transcripts into higher-order granules. These higher-order granules may form by fusion of smaller homotypic granules and indeed fusion of granules labeled with GFP-Vas is observed by live imaging[23]. Alternatively, clusters of different mRNAs may grow alongside each other on a predefined granule scaffold. The localization of *C. elegans* germ granules – P granules – occurs via a phase transition in which soluble RNP components condense at the posterior of the embryo[36]. It is interesting to consider whether formation of homotypic clusters occurs by a condensation of single transcript RNPs mediated by RNA-binding proteins.

In contrast to other posteriorly localized RNAs, which travel as single molecules, *osk* forms oligomeric complexes beginning in the nurse cells. Previous studies indicated that reporters containing the *osk* 3′UTR can hitchhike on wild-type *osk* mRNA by 3′UTR-mediated dimerization[8,37]. Hitchhiking is not required for *osk* transport, but co-packaging may be important for translational repression of *osk* prior to localization[27,28]. Consistent with this, multi-copy RNPs are competent for localization by both kinesin-dependent transport during mid-oogenesis and diffusion/entrapment during late stages of oogenesis.

Previous ISH-immuno-electron microscopy analysis of stage 10 oocytes showed co-localization of *osk* with Stau, but not with Osk protein in polar granules[38] and our results indicate that *osk*/Stau RNPs are continuously segregated from the germ plasm granules. This physical separation has functional consequences. Whereas co-packaging of *nos*, *pgc*, and *cycB* coordinates their transport to posterior nuclei and consequent segregation to the pole cells, *osk* is specifically excluded. Although we do not know why targeting of Osk to polar granules appears to alter their function, it is clearly detrimental to germline development. It will be interesting to determine whether *osk*/Stau granules contain other mRNAs whose functions are required specifically during oogenesis or early embryogenesis but must be excluded from pole cells.

METHODS

Fly stocks

The following mutants, mutant combinations, and transgenic lines were used: *y* w^{67c23} (ref. [39]); osk^{A87} (ref [40]); vas^{PD}/vas^{D1} (ref. [41,42]); nos^{BN} (ref. [43]); *nos*-$(ms2)_{18}$ (ref. [44]); *osk*-$(ms2)_6$ (ref. [45]); *hsp83-MCP-GFP* (ref. [16]); *gfp-stau* (ref. [46]); *gfp-vas* (ref. [47]); *osk-gfp* (ref. [48]); *osk-bcd3′UTR* (ref. [30]). *UASp-oskΔi1,2-nos3′UTR* was created by standard molecular biology methods and introduced into *y* w^{67c23} animals by P element-mediated transformation (ref. [49]). The *UASp-gfp-nos3′UTR* transgenic line was kindly provided by W. Eagle. Expression was elicited in heterozygous females using the maternal triple Gal4 driver (*MTD-Gal4*, ref. [50]).

Single molecule FISH

FISH was performed as previously described[20] using oligonucleotides 20 nt in length and complementary to transcripts *nos*-RA (CG5637; 75 probes), *cycB*-RA (CG3510; 48 probes), *pgc*-RA (CG32885; 48 probes), and *osk*-RA (CG10901; 99 probes). Sequences are listed in

Supplementary Table 1. Custom oligonucleotides with 3′ amine modification were obtained from Biosearch Technologies, conjugated to either Atto 565 (Sigma 72464) or Atto 633 (Sigma 43429) dye, and purified by HPLC as previously described[51]. Intact ovaries were dissected from well-fed 2–4 day old females and processed for FISH as described[23]. Imaging was performed using a 63x HCX PL APO CS 1.4 NA oil immersion objective on a Leica TCS SP5 laser-scanning confocal microscope equipped with GaAsP "HyD" detectors in photon counting mode, with pixels of 76 x 76 nm and z spacing of 340 nm. For each probe set, laser power was adjusted to optimize separation of signal and noise. The same settings were used repeatedly for all samples treated with a given probe set. For each experiment, image stacks were acquired from 3–5 different egg chambers/oocytes or embryos at each developmental stage shown. Each stack contained 20,000–100,000 particles, depending on the volume imaged and the size of the egg chamber/oocyte/embryo. Laser power exhibited fluctuations of ~10% between experiments; however, normalization to single mRNA intensity nullifies any effect in our measurements of absolute mRNA amount. For egg chambers/oocytes, z-series represent approximately half the thickness of the tissue starting from near the interface between the follicle cells and the nurse cells/oocyte. For embryos, image stacks extend from the cortical surface to near the midsagittal plane.

As controls for goodness of single particle detection, we compared the densities of punctae in early embryos from wild-type females and from females heterozygous or homozygous for the maternal RNA-null nos^{BN} allele. As expected, heterozygous embryos contain half as many particles as in wild-type (0.39 ± 0.01 versus 0.75 ± 0.02 particles/μm^3, n = 4 embryos each). In homozygous nos^{BN} embryos, the number of particles/volume exceeding the "difference of Gaussians" detection threshold[52] was <1% of the number detected in wild-type. Similarly for *osk*, embryos from females heterozygous for the mRNA-null allele osk^{A87} contain half the number of particles of wild-type embryos (0.24 ± 0.03 versus 0.41 ± 0.03 particles/μm^3 in wild-type, n = 4 embryos each). These results are similar to the two-fold reduction in particle number observed for maternally supplied *hunchback* (*hb*) mRNA in *hb* deficiency heterozygotes[20] and support previous findings[20,21] that the FISH method effectively distinguishes true objects from imaging noise.

Immunostaining

For pole cell counting, anti-Vas immunofluorescence was performed on 1–3 hr old embryos as described[53] using 1:2000 rabbit anti-Vas (gift of P. Lasko) and 1:1000 Alexa Fluor–568 goat anti-rabbit secondary antibody (Molecular Probes). Images were taken at 2.5 μm intervals throughout the embryo posterior with a Leica TCS SP5 confocal microscope using a 20x objective. For gonad analysis, anti-Vas staining of 6–16 hour old embryos was followed by 1:2000 biotin goat anti-mouse (Jackson ImmunoResearch) secondary antibody, amplification with Vectastain reagent (Vector Labs), and peroxidase immunohistochemistry. Embryos were mounted in Aquapolymount and imaged using Nomarski optics.

Absolute RT-qPCR mRNA quantification and comparison to image particle counts

RT-qPCR was performed on individual embryos isolated from embryos 0–30 min after egg deposition as described[20]. The following PCR primers were used: *nos* (5′-

GTGCGAGTCACCAGCAAACGGACG-3′ and 5′-CGTAGGACATGCGACCGAGATCATCG-3′); *osk* (5′-CAACGAAAGGGGCGTGGTGCG-3′ and (5′-CGCTGCCGACCGATTTTGTTCCAG-3′). DNA standard curves were generated using the *nos* N5 (ref. [54]) or Blue-osk[55] cDNA plasmids; RNA standard curves were generated using template mRNA prepared by in vitro transcription of the corresponding plasmid with the mMessage mMachine T7 kit (Ambion). Fractional recovery of mRNA from processed embryos is estimated at about 30% (ref. [20,21]).

The mean number of *nos* transcripts measured by RT-qPCR ($2.5 \pm 0.4 \times 10^6$, n = 6 embryos) was compared to the total number of particles detected in tiled confocal stacks representing the left or right halves of 4 embryos ($2.0 \pm 0.5 \times 10^6$). Previous work has shown that 4% of *nos* mRNA is posteriorly localized[22]. Thus, although these transcripts are underrepresented in the total number of particles counted but not in the RT-qPCR measurement, a discrepancy of 4% is significantly smaller than the inherent measurement errors (16% for RT-qPCR, 25% for particle counting). The discrepancy between the number of particles and the number of transcripts reflects the probability that multiple mRNAs occupy the same imaging volume by random chance (see below). We conclude that most unlocalized *nos* particles observed by imaging correspond to individual mRNAs. The intensity distributions and densities of *cycB* and *pgc* are highly similar to those of *nos* in our experiments, consistent with the idea that the unlocalized transcripts do not form multi-copy complexes.

The mean number of *osk* mRNAs measured by RT-qPCR ($1.9 \pm 0.6 \times 10^6$, n = 6 embryos) was compared to the total number of particles counted in tiled confocal stacks covering the left or right halves of 4 embryos ($0.9 \times 10^6 \pm 0.4$ *osk* particles per embryo). From these measurements, the average *osk* particle contains 2.1 ± 1.1 mRNAs. Previous work has estimated that 18% of *osk* is found at the posterior pole[22], a substantially larger fraction than for *nos*. Examining particle intensity and spatial distributions, we estimate that at least 95% of particles are not localized at the posterior pole. Since these must account for 82% of *osk* mRNA, we find that the average unlocalized particle contains (0.82 x 1.9) / (0.95 x 0.9) = 1.8 mRNAs. This value is consistent with the estimated frequency of co-localization of 2 or more *osk* mRNAs (see below and Supplementary Fig. 5d). In these estimates, 40% of particles contain 1 mRNA, 50% contain 2 mRNAs, and 10% 4 mRNAs. This yields a mean mRNA content per particle (0.4 x 1) + (0.5 x 2) + (0.1 x 4) = 1.8. We conclude that FISH is capable of distinguishing individual *osk* mRNAs.

For all FISH results, the fixation, in situ hybridization, and mounting processes lead to reduction in embryo length by up to 15% and compression along the imaging axis by 30%. Therefore, living embryos will exhibit distances that are larger, and densities that are lower, than the values we report for fixed samples.

Estimation of spurious co-localization

If individual mRNAs are scattered within a volume at random, then two or more mRNAs may occupy the same confocal imaging volume purely by chance. Such spurious co-localization will result in mis-detection of two mRNAs as a single object with an mRNA content of two mRNAs, erroneously appearing to represent a multi-copy particle. The rate of

spurious co-localization depends on the density of mRNAs. To determine whether the observed frequency of *nos* co-localization exceeds the frequency expected for random chance, we utilized two methods: first, we developed a simple Poissonian model of random co-localization; second, we constructed pair-correlation functions.

Model of random co-localization—A simple model of random co-localization can predict the frequency of spurious co-localization. The model requires choosing an effective volume occupied by diffraction-limited spots in confocal microscopy, with the assumption that when random co-localization occurs, two or more mRNAs inhabit the same position within an imaging volume and are always mis-detected as 1 particle (and never correctly detected as 2 particles). In reality, our algorithm fails gradually, rather than abruptly, to discriminate between two closely spaced particles as the distances between the particles decrease. To bias our estimates toward the hypothesis that packaging does indeed occur for unlocalized *nos*, we intentionally used small effective volumes and chose high mRNA densities at which we fail to distinguish individual mRNAs.

In the first estimate, we assumed that diffraction limited spots have a volume of $\frac{4}{3}\pi(0.3 \times 0.3 \times 0.9\,\mu\mathrm{m}) = 0.35\,\mu\mathrm{m}^3$ where, as observed previously with the same imaging protocol, the radius along the z-axis is about 3-fold higher than in the xy plane of the image[20]. At a density of 0.8 particles/μm^3 x 1.3 mRNA/particle = 1.0 mRNA/μm^3, unlocalized *nos* mRNA occupies, on average, 1.0 mRNA/μm^3 x 0.35 μm^3/mRNA = 35% of available volume. With this mean occupancy rate, the Poisson distribution was used to predict the fraction of imaging volumes containing n = 0, 1, 2… mRNAs (Supplementary Fig. 1f), assuming that detected particles contain an integer number of mRNAs. Of the total volumes with n > 0 (that is, for all detected particles), the fractions with n = (1, 2, 3) are p = (0.83, 0.15, 0.02) and the fraction of volumes with n ≥ 4 is negligible (Supplementary Fig. 1f inset). This predicts that about 1 – 0.83 = 17% of detected *nos* punctae represent more than one mRNA that co-localize by random chance. This prediction is consistent with the distribution of normalized intensities of 55,744 particles in a 2D histogram (Fig. 1e,f): the distribution along the correlated axis can be approximated by the sum of a pair of Gaussians centered on means of 1 and 2 mRNAs with standard deviations of 0.28 and $\sqrt{2 \times 0.28^2} = 0.40\,\mathrm{mRNAs}$, since variances of the intensities of two mRNAs are additive. With these fits, the ratio of the area under the Gaussian with mean = 2 to that with mean = 1 mRNA in Fig. 1f is 20% ± 3%, or 9291 ± 1932 co-localized particles. This is close to the prediction from the Poisson model of p(n = 2) / p(n = 1) = 0.15 / 0.83 = 18%. Moreover, the predicted probabilities closely recapitulate the measured mean particle content: [1 mRNA x p(n=1)] + [2 mRNA x p(n=2)] + [3 mRNA x p(n=3)] = 0.83 + 0.3 + 0.06 = 1.2 mRNA/particle, similar to the measured value of 1.3 mRNA/particle. This supports the idea that co-localization of two or more unlocalized *nos* mRNAs arises by random chance alone.

In the above estimate, mis-detection of 2 mRNAs as 1 occurs when the two centroids are separated by ≤0.6 μm in the xy plane. In reality, the algorithm becomes gradually less successful at discriminating two objects as the distance between centroids decreases. Thus, the degree of purely spurious co-localization might be smaller than estimated above. We can make a second estimate that compensates for this effect by using a smaller volume of a

diffraction limited spot of $\frac{4}{3}\pi(0.25 \times 0.25 \times 0.75\,\mu\mathrm{m}) = 0.2\,\mu\mathrm{m}^3$. In this case, the mRNA will occupy 20% of the available volume, leading to a predicted spurious co-localization frequency of 10%. Given our estimate from Fig. 1f the co-localization of unlocalized *nos* mRNAs is ~20%, the remaining 10% of co-localization would occur for non-random reasons, i.e. deliberate packaging of two or three *nos* mRNAs into the same RNP. However, we note that mRNAs are not randomly scattered with equal probability at all locations throughout the embryo interior. Examination of image stacks shows that a large fraction (possibly as high as 50%) of the embryo is devoid of mRNAs Supplementary (Fig. 1g), likely because of the presence of organelles, yolk granules, or other structures. This results in more dense crowding of mRNAs than expected (Supplementary Fig. 1g). Thus, the effective density of *nos* mRNA is >1/μm^3, increasing the probability of spurious co-localization. Indeed, in two-color FISH images where one channel is rotated 90° relative to the other, the probability of co-detection of unlocalized particles is only about 10% (Supplementary Fig. 1h), consistent with the idea that *nos* is excluded from some regions of the embryo. If *nos* were excluded from 40% of the embryo volume, this would effectively increase the density of unlocalized material to 1 mRNA/0.6 μm^3 = 1.7 mRNA/μm^3. This density, if used in combination with a smaller particle volume, predicts mean mRNA content of 1.7 mRNA/μm^3 x 0.2 μm^3/mRNA = 34%, again giving rise in the Poisson model (Supplementary Fig. 1i) to values similar to the observed distributions in Fig. 1g. Thus, for *nos*, random co-localization of individual mRNAs in the same confocal imaging volume is the most parsimonious explanation for the fraction of unlocalized punctae that contain 2 mRNAs.

The same reasoning can be used to assess the likelihood that unlocalized *osk* mRNAs are found in dimeric complexes: the density of unlocalized *osk* particles is lower than for *nos*, at 0.4/μm^3. Our imaging and analysis algorithm is capable of distinguishing nearly all particles at this density[20]. *osk* mRNA is present at a density of 0.4 particles/μm^3 x 1.8 mRNAs/particle = 0.7 mRNA/μm^3. At this density, mRNA is expected to occupy 25% of the available volume, and so the predicted rate of co-localization of 2 or more mRNAs by random chance is 12%, 5-fold lower than the 60% estimated from observations (Supplementary Fig. 5d). Since random co-localization dramatically fails to account for the fraction of unlocalized punctae containing >1 mRNA, we conclude that unlocalized *osk* is deliberately packaged into higher-order RNP complexes containing 2 or more mRNAs.

Pair-correlation analysis—We constructed pair-correlation functions by measuring the density of *nos* and *pgc* as a function of distance from a set of “reference” *nos* particles. In determining *nos* densities, we considered 18% of detected *nos* particles to represent 2 mRNAs at the same coordinates. We observed no significant change in density of either *nos* or *pgc* as a function of distance from reference particles (Supplementary Fig. 1j), as expected if co-localization in bulk cytoplasm occurs by random chance alone.

mRNA content of localized granules

Particle fluorescence intensities and offsets were estimated by three methods: 2D elliptical Gaussian fitting[52], summation of fluorescence in a circular area with radius of 3 pixels (for amplitude) and in a ring with inner radius 6 pixels and outer radius 9 pixels (for offset), and

3D summation as previously described for sites of zygotic gene expression[20]. The fluorescence intensity value for a single mRNA molecule was estimated by two methods: 1) constructing an average image of an unlocalized single-copy particle and either fitting an elliptical Gaussian to obtain an amplitude and offset or summing fluorescence in 2D; 2) analyzing unlocalized particles within a volume of cytoplasm in the interior of the oocyte or embryo below the posterior cortex. In this region, particle density decreases approaching the posterior pole (Supplementary Fig. 1b), and particle density and fluorescence are roughly linearly related. The slope of a line fit to a plot of total intensity as a function of particle number yields fluorescence per particle[20]. Normalization of granule intensity to fluorescence per single-copy particle yields absolute mRNA content per granule. In pairwise comparisons, the three analysis methods yielded mRNA counts that differed by a maximum of 20% for granules localized at the posterior cortex. This measurement error was considerably higher (up to 60%) for granules positioned less than 5 μm from the posterior pole.

Time-lapse movies of oocytes expressing *nos**GFP or *osk**GFP were obtained as previously described[23] from n = 3 (*nos**GFP) or n = 4 (*osk**GFP) oocytes. Granules were tracked using semi-automated custom software[23]. Average velocities were calculated for 26 (*nos*) and 22 (*osk*) granules. Relative fluorescence intensities were obtained from >250 granules each via 2D summation, and histograms of granule intensities were fit to histograms of FISH intensities of a subset of granules found in a region of the posterior cortex comparable to the region visualized by time-lapse imaging. Histograms of granules observed in time-lapse images do not show a clear threshold separating true particles from imaging noise, so the fit was performed to the right side of the FISH distribution under the assumption that dim particles are not visible in time-lapse images. Fitting was performed to minimize chi square error over a range of bin sizes and minimum and maximum intensity values.

Supplementary Material

Refer to Web version on PubMed Central for supplementary material.

Acknowledgments

We thank W. Eagle, P. Lasko, P. Macdonald, and D. St Johnston for fly stocks and reagents, S. Chatterjee and S. Kyin for technical assistance, and E. Abbaszadeh, S. Blythe, and B. He for comments on the manuscript. This work was funded by National Institute of Health grant R01GM067758 (E.R.G) and the Howard Hughes Medical Institute (E.F.W.).

References

1. Pratt CA, Mowry KL. Taking a cellular road-trip: mRNA transport and anchoring. Curr Opin Cell Biol. 2013; 25:99–106. [PubMed: 23200723]
2. Marchand V, Gaspar I, Ephrussi A. An intracellular transmission control protocol: assembly and transport of ribonucleoprotein complexes. Curr Opin Cell Biol. 2012; 24:202–210. [PubMed: 22278045]
3. Lange S, et al. Simultaneous transport of different localized mRNA species revealed by live-cell imaging. Traffic. 2008; 9:1256–1267. [PubMed: 18485054]

4. Amrute-Nayak M, Bullock SL. Single-molecule assays reveal that RNA localization signals regulate dynein-dynactin copy number on individual transcript cargoes. Nat Cell Biol. 2012; 14:416–423. [PubMed: 22366687]
5. Tubing F, et al. Dendritically localized transcripts are sorted into distinct ribonucleoprotein particles that display fast directional motility along dendrites of hippocampal neurons. J Neurosci. 2010; 30:4160–4170. [PubMed: 20237286]
6. Mikl M, Vendra G, Doyle M, Kiebler MA. RNA localization in neurite morphogenesis and synaptic regulation: current evidence and novel approaches. J Comp Physiol. 2010; 196:321–334. [PubMed: 20237785]
7. Batish M, van den Bogaard P, Kramer FR, Tyagi S. Neuronal mRNAs travel singly into dendrites. Proc Natl Acad Sci USA. 2012; 109:4645–4650. [PubMed: 22392993]
8. Jambor H, Brunel C, Ephrussi A. Dimerization of *oskar* 3′ UTRs promotes hitchhiking for RNA localization in the *Drosophila* oocyte. RNA. 2011; 17:2049–2057. [PubMed: 22028360]
9. Mahowald AP. Assembly of the *Drosophila* germ plasm. Int Rev Cytol. 2001; 203:187–213. [PubMed: 11131516]
10. Rangan P, et al. Temporal and spatial control of germ-plasm RNAs. Curr Biol. 2009; 19:72–77. [PubMed: 19110432]
11. Lecuyer E, et al. Global analysis of mRNA localization reveals a prominent role in organizing cellular architecture and function. Cell. 2007; 131:174–187. [PubMed: 17923096]
12. Cinalli RM, Rangan P, Lehmann R. Germ cells are forever. Cell. 2008; 132:559–562. [PubMed: 18295574]
13. Nakamura A, Seydoux G. Less is more: specification of the germline by transcriptional repression. Development. 2008; 135:3817–3827. [PubMed: 18997110]
14. Becalska AN, Gavis ER. Lighting up mRNA localization in *Drosophila* oogenesis. Development. 2009; 136:2493–2503. [PubMed: 19592573]
15. Sinsimer KS, Jain RA, Chatterjee S, Gavis ER. A late phase of germ plasm accumulation during *Drosophila* oogenesis requires Lost and Rumpelstiltskin. Development. 2011; 138:3431–3440. [PubMed: 21752933]
16. Forrest KM, Gavis ER. Live imaging of endogenous mRNA reveals a diffusion and entrapment mechanism for *nanos* mRNA localization in *Drosophila*. Curr Biol. 2003; 13:1159–1168. [PubMed: 12867026]
17. Dalby B, Glover DM. 3′ non-translated sequences in *Drosophila* cyclin B transcripts direct posterior pole accumulation late in oogenesis and peri-nuclear association in syncytial embryos. Development. 1992; 115:989–997. [PubMed: 1451670]
18. Nakamura A, Amikura R, Mukai M, Kobayashi S, Lasko P. Requirement for a noncoding RNA in *Drosophila* polar granules for germ cell establishment. Science. 1996; 274:2075–2079. [PubMed: 8953037]
19. Lerit DA, Gavis ER. Transport of germ plasm on astral microtubules directs germ cell development in *Drosophila*. Curr Biol. 2011; 21:439–448. [PubMed: 21376599]
20. Little SC, Tikhonov M, Gregor T. Precise developmental gene expression arises from globally stochastic transcriptional activity. Cell. 2013; 154:789–800. [PubMed: 23953111]
21. Petkova MD, Little SC, Liu F, Gregor T. Maternal origins of developmental reproducibility. Curr Biol. 2014; 24:1283–1288. [PubMed: 24856210]
22. Bergsten SE, Gavis ER. Role for mRNA localization in translational activation but not spatial restriction of *nanos* RNA. Development. 1999; 126:659–669. [PubMed: 9895314]
23. Sinsimer KS, Lee JJ, Thiberge SY, Gavis ER. Germ plasm anchoring is a dynamic state that requires persistent trafficking. Cell reports. 2013; 5:1169–1177. [PubMed: 24290763]
24. Zimyanin VL, et al. In vivo imaging of *oskar* mRNA transport reveals the mechanism of posterior localization. Cell. 2008; 134:843–853. [PubMed: 18775316]
25. Micklem DR, Adams J, Grunert S, St Johnston D. Distinct roles of two conserved Staufen domains in *oskar* mRNA localization and translation. EMBO J. 2000; 19:1366–1277. [PubMed: 10716936]
26. Rongo C, Gavis ER, Lehmann R. Localization of *oskar* RNA regulates *oskar* translation and requires Oskar protein. Development. 1995; 121:2737–2746. [PubMed: 7555702]

27. Chekulaeva M, Hentze MW, Ephrussi A. Bruno acts as a dual repressor of *oskar* translation, promoting mRNA oligomerization and formation of silencing particles. Cell. 2006; 124:521–533. [PubMed: 16469699]
28. Besse F, Lopez de Quinto S, Marchand V, Trucco A, Ephrussi A. *Drosophila* PTB promotes formation of high-order RNP particles and represses *oskar* translation. Genes Dev. 2009; 23:195–207. [PubMed: 19131435]
29. Glotzer JB, Saffrich R, Glotzer M, Ephrussi A. Cytoplasmic flows localize injected *oskar* RNA in Drosophila oocytes. Curr Biol. 1997; 7:326–337. [PubMed: 9115398]
30. Ephrussi A, Lehmann R. Induction of germ cell formation by *oskar*. Nature. 1992; 358:387–392. [PubMed: 1641021]
31. Ghosh S, Marchand V, Gaspar I, Ephrussi A. Control of RNP motility and localization by a splicing-dependent structure in *oskar* mRNA. Nat Struct Mol Biol. 2012; 19:441–449. [PubMed: 22426546]
32. Gavis ER, Curtis D, Lehmann R. Identification of cis-acting sequences that control *nanos* RNA localization. Dev Biol. 1996; 176:36–50. [PubMed: 8654893]
33. Smith JL, Wilson JE, Macdonald PM. Overexpression of *oskar* directs ectopic activation of *nanos* and presumptive pole cell formation in *Drosophila* embryos. Cell. 1992; 70:849–859. [PubMed: 1516136]
34. Koch AL. The logarithm in biology. 1. Mechanisms generating the log-normal distribution exactly. Journal of theoretical biology. 1966; 12:276–290. [PubMed: 5972197]
35. Limpert E, Stahel WA, Abbt M. Log-normal distributions across the sciences: keys and clues. Bioscience. 2001; 51:341–352.
36. Brangwynne CP, et al. Germline P granules are liquid droplets that localize by controlled dissolution/condensation. Science. 2009; 324:1729–1732. [PubMed: 19460965]
37. Hachet O, Ephrussi A. Splicing of *oskar* RNA in the nucleus is coupled to its cytoplasmic localization. Nature. 2004; 428:959–963. [PubMed: 15118729]
38. Herpers B, Xanthakis D, Rabouille C. ISH-IEM: a sensitive method to detect endogenous mRNAs at the ultrastructural level. Nat Protocols. 2010; 5:678–687. [PubMed: 20360763]
39. Lindsley, DL.; Zimm, GG. The genome of Drosophila melanogaster. Academic Press, Inc; San Diego: 1992.
40. Vanzo NF, Ephrussi A. Oskar anchoring restricts pole plasm formation to the posterior of the *Drosophila* oocyte. Development. 2002; 129:3705–3714. [PubMed: 12117819]
41. Lehmann R, Nusslein-Volhard C. The maternal gene *nanos* has a central role in posterior pattern formation of the *Drosophila* embryo. Development. 1991; 112:679–691. [PubMed: 1935684]
42. Schüpbach T, Wieschaus E. Maternal-effect mutations altering the anterior-posterior pattern of the *Drosophila* embryo. W Roux's Arch Dev Biol. 1986; 195:302–317.
43. Wang C, Dickinson LK, Lehmann R. Genetics of *nanos* localization in *Drosophila*. Dev Dynam. 1994; 199:103–115.
44. Brechbiel JL, Gavis ER. Spatial regulation of *nanos* is required for its function in dendrite morphogenesis. Curr Biol. 2008; 18:745–750. [PubMed: 18472422]
45. Lin MD, Fan SJ, Hsu WS, Chou TB. *Drosophila* decapping protein 1, dDcp1, is a component of the *oskar* mRNP complex and directs its posterior localization in the oocyte. Dev Cell. 2006; 10:601–613. [PubMed: 16678775]
46. Martin SG, Leclerc V, Smith-Litiere K, St Johnston D. The identification of novel genes required for *Drosophila* anteroposterior axis formation in a germline clone screen using GFP-Staufen. Development. 2003; 130:4201–4215. [PubMed: 12874138]
47. Johnstone O, Lasko P. Interaction with eIF5B is essential for Vasa function during development. Development. 2004; 131:4167–4178. [PubMed: 15280213]
48. Snee MJ, Harrison D, Yan N, Macdonald PM. A late phase of Oskar accumulation is crucial for posterior patterning of the *Drosophila* embryo, and is blocked by ectopic expression of Bruno. Differentiation. 2007; 75:246–255. [PubMed: 17359300]
49. Spradling, AC. P element-mediated transformation. In: Roberts, DB., editor. Drosophila: A Practical Approach. IRL Press; Oxford: 1986. p. 175-197.

50. Petrella LN, Smith-Leiker T, Cooley L. The Ovhts polyprotein is cleaved to produce fusome and ring canal proteins required for *Drosophila* oogenesis. Development. 2007; 134:703–712. [PubMed: 17215303]

51. Raj A, van den Bogaard P, Rifkin SA, van Oudenaarden A, Tyagi S. Imaging individual mRNA molecules using multiple singly labeled probes. Nat Methods. 2008; 5:877–879. [PubMed: 18806792]

52. Little SC, Tkacik G, Kneeland TB, Wieschaus EF, Gregor T. The formation of the Bicoid morphogen gradient requires protein movement from anteriorly localized mRNA. PLoS Biol. 2011; 9:e1000596. [PubMed: 21390295]

53. Duchow HK, Brechbiel JL, Chatterjee S, Gavis ER. The *nanos* translational control element represses translation in somatic cells by a Bearded box-like motif. Dev Biol. 2005; 282:207–217. [PubMed: 15936341]

54. Wang C, Lehmann R. *Nanos* is the localized posterior determinant in Drosophila. Cell. 1991; 66:637–647. [PubMed: 1908748]

55. Ephrussi A, Dickinson LK, Lehmann R. *oskar* organizes the germ plasm and directs localization of the posterior determinant *nanos*. Cell. 1991; 66:37–50. [PubMed: 2070417]

56. Spradling, AC. Developmental genetics of oogenesis. In: Bate, M.; Martinez Arias, A., editors. The Development of Drosophila melanogaster. Vol. I. Cold Spring Harbor Press; Cold Spring Harbor: 1993. p. 1-70.

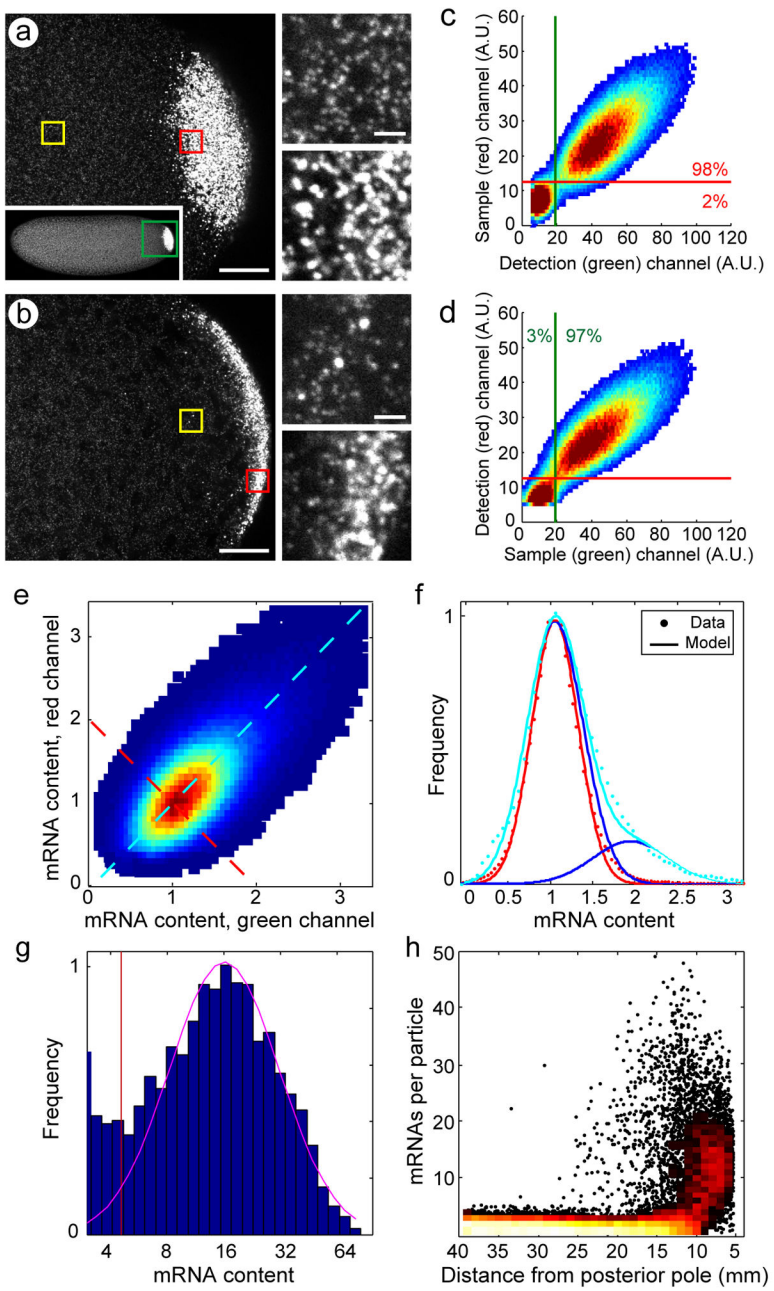

Figure 1. Measuring absolute mRNA content of *nos* granules

(a,b) Confocal section near the cortical surface (**a**) or near the mid-sagittal plane (**b**) of an early, nuclear cycle (n.c.) 3 embryo (anterior left, dorsal up) labeled with *nos* probes (**a**; green box in inset shows region displayed in main panel). Right panels show magnified views of regions indicated by yellow (right upper panels) and red (right lower panels) boxes. Scale bars: 20 μm (left panels); 2 μm (right panels). **(c,d)** Detection efficiency of unlocalized *nos* particles in two-color FISH using *nos* probes with alternating fluorophores. Particles are detected in one channel (“Detection channel”) on the basis of separation from imaging noise, then intensity measurements are made in the second channel (“Sample channel”) at

the same positions. Plots show 2D histograms where color indicates relative density of data points. Red horizontal and green vertical lines represent detection thresholds separating true objects from imaging noise. Percentages indicate fraction of objects found in the sample channel that fall above or below the threshold in the detection channel. (**e)** 2D histogram shows a weak correlation for normalized mRNA content of unlocalized particles. Cyan and red dashed lines indicate correlated and anticorrelated axes, respectively, through the point (1,1). (**f)** Cross-sections through histogram shown in (**e**) along correlated (cyan) and anticorrelated (red) axes. Circles indicate data points. A single Gaussian distribution fits experimental observations along the anticorrelated axis (red), whereas the distribution along the correlated axis is approximated by the sum (cyan line) of two Gaussians (blue lines) with means of 1 and 2 mRNAs (see also Supplementary Fig. 1). (**g)** Log-normal distribution of *nos* mRNA content in localized granules (separated from unlocalized punctae by vertical red line). (**h)** mRNA content as a function of distance from the posterior pole. Heat map indicates relative density of data points (see also Supplementary Fig. 1j).

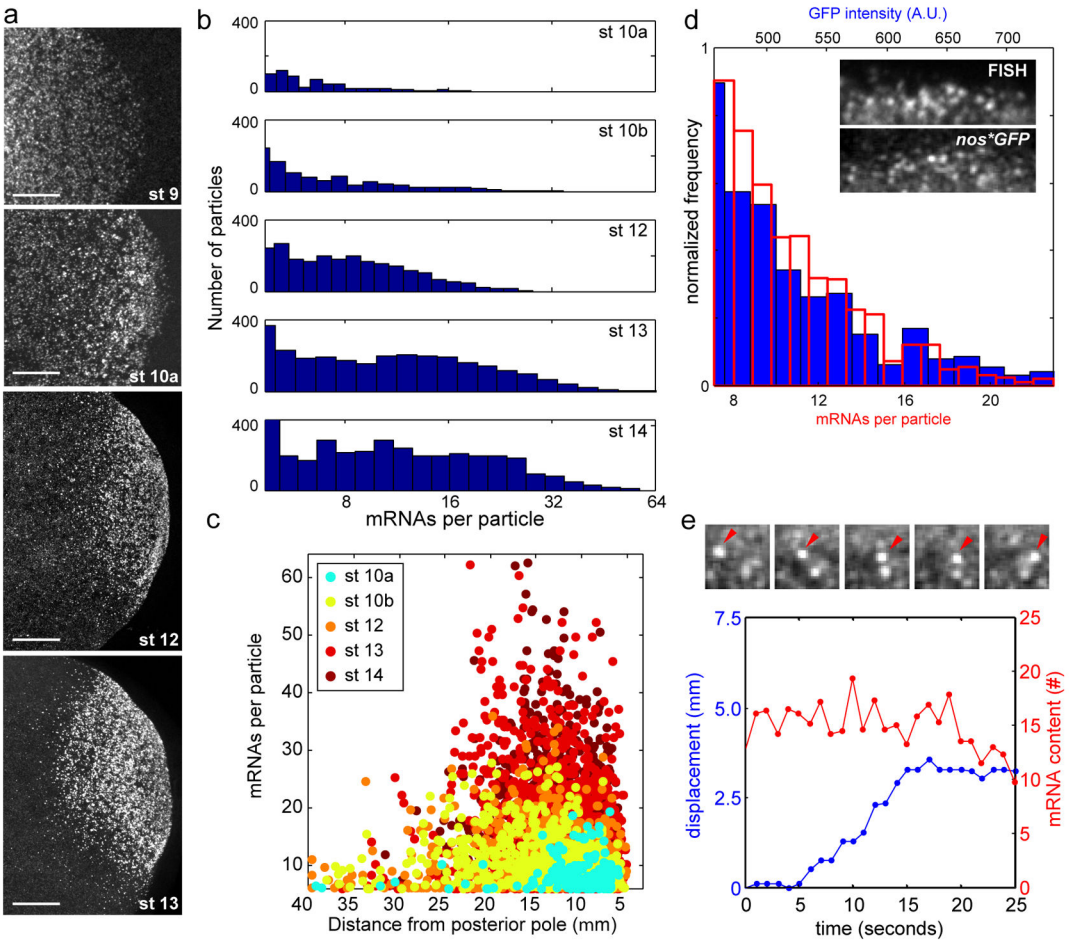

Figure 2. *nos* granule assembly occurs exclusively at the posterior oocyte cortex

(a) Maximum z-series projections spanning 5 μm at the posterior oocyte cortex show the extent of *nos* localization at four different stages of oogenesis. Scale bars: 10 μm (stage 9, 10a); 20 μm (stage 12, 13). (**b)** Distributions of *nos* mRNA content per granule during late oogenesis (also see Supplementary Fig. 2). (**c)** *nos* content as a function of distance from the posterior pole. (**d)** Calibration of intensity distributions of *nos**GFP granules in time-lapse movies (solid blue bars; arbitrary units) to FISH granules (red outline, absolute mRNA number). Inset depicts one frame of a *nos**GFP time-lapse movie compared to a FISH image. (**e)** An individual granule (arrowhead) containing approximately 15 mRNAs travels ~3 μm in 10 sec while maintaining *nos* content. Frames correspond to times t = 4, 7, 10, 12, and 15 sec. Displacement (blue) is calculated as root-mean-square distance from the t = 0 position. Fluctuations in mRNA content (red) centered on ~15 mRNAs result from imaging noise (see also Supplementary Fig. 2).

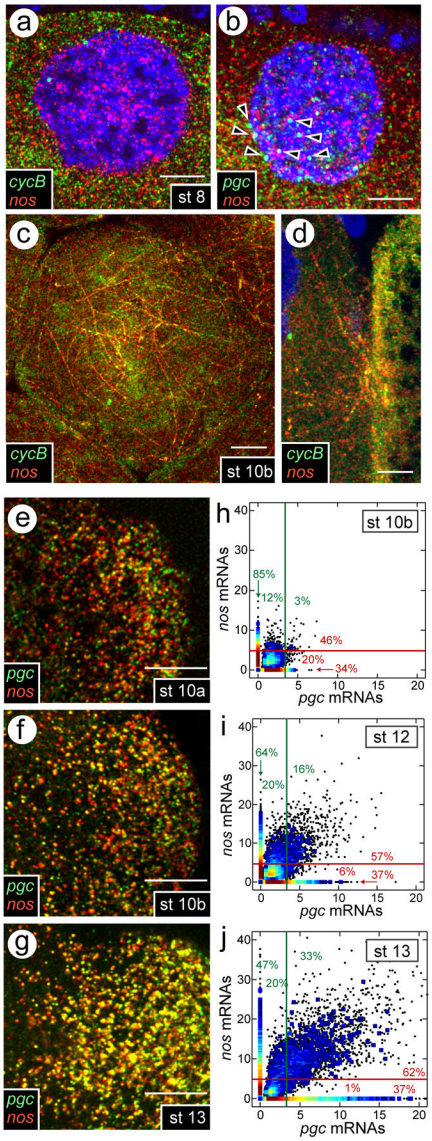

Figure 3. Co-localization of polar granule components begins during late oogenesis

(**a–d**) Detection of *nos*, *pgc*, and *cycB* in nurse cells by FISH. (**a,b**) Confocal sections of nurse cells at stage 8. *nos*, *pgc*, and *cycB* are found in separate particles (also see Supplementary Fig. 3). In some instances, putative sites of nascent transcription cluster to one side of a nurse cell nucleus (arrowheads in **b**) and this is often associated with enrichment of single mRNAs in the cytoplasm closest to the transcription sites; additional sites are present in adjacent z sections. (**c,d**) Maximum z-series projections spanning 5 μm at stage 10b near the cortex (**c**) and near a putative ring canal leading to the oocyte (**d**) showing filamentous networks enriched for these RNPs. Blue: DAPI staining. Scale bars: 10 μm. (**e–g**) Maximum z-series projections over 5 μm of the posterior oocyte cortex. *pgc* and *nos* are first detected in posterior granules at stage 10a (**e**) and are often enriched in the same granule (**f**: stage 10b; **g**: stage 13). Scale bars: 5 μm (**e,f**); 10 μm (**g**). (**h–j**) 2D histograms of *nos* and *pgc* content in all detected particles at stage 10b (**h**), stage 12 (**i**), and stage 13 (**j**).

Heat map indicates relative density of data points. Horizontal red and vertical green lines indicate thresholds separating localized granules and unlocalized particles. For all localized granules detected above the threshold in one channel (to the right of the green line for localized *pgc*; above the red line for localized *nos*), percentages indicate the fractions with zero content, low content (primarily unlocalized particles), or high content (corresponding to localized granules) in the second channel (as read from left to right for *nos* in green; from top to bottom for localized *pgc* in red). *cycB* behaves similarly to *nos* and *pgc* (see Supplementary Fig. 3).

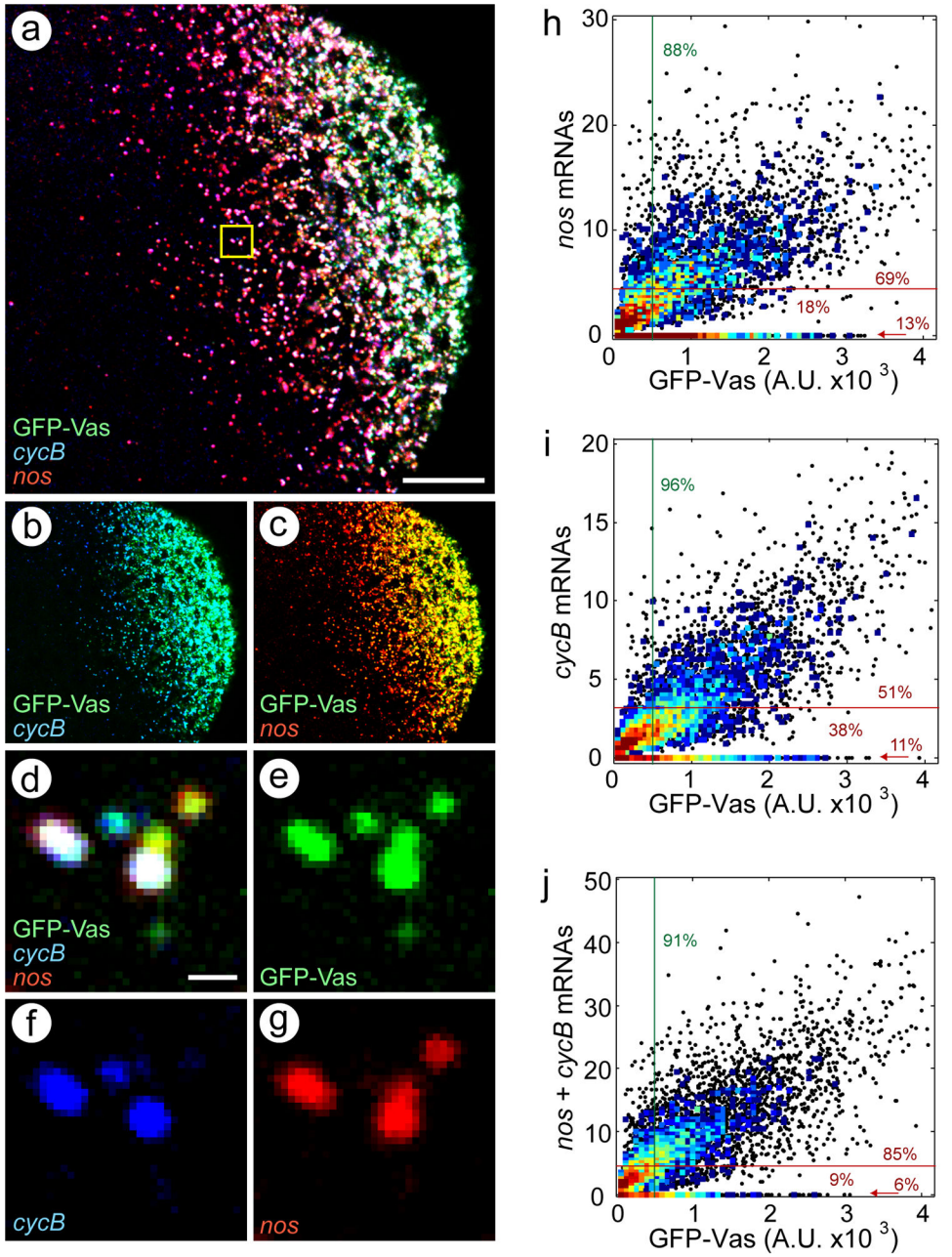

Figure 4. mRNA content of posterior granules is heterogeneous

(**a–g)** Maximum z-series projections spanning 8 μm at the posterior cortex of a stage 13 GFP-Vas oocyte co-labeled with probes for *nos* and *cycB*. (**a**) Merge of all three channels. (**b,c**) Pairs of channels illustrate a high degree of co-localization between GFP-Vas and *cycB* (**b**) or *nos* (**c**). (**d–g**) An enlarged view of the boxed area in (**a**) shows heterogeneity of granule components. Scale bars: 10 μm (**a**); 0.5 μm (**d–g**). (**h–j)** 2D histograms of GFP-Vas fluorescence in arbitrary units (A.U.) and the number of *nos* (**h**), *cycB* (**i**), or *nos*+*cycB* (**j**) mRNAs per granule. Horizontal red lines indicate the threshold separating localized and unlocalized particles by mRNA content. Vertical green lines represent the threshold between

readily distinguished GFP-Vas granules and imaging noise. 13% of GFP-Vas granules contain 0 *nos* mRNAs and 11% contain 0 *cycB*. Conversely, at least 88% of localized *nos* and 96% of localized *cycB* granules contain GFP-Vas. A small fraction (6%) of posteriorly localized GFP-Vas granules contain neither mRNA (**j**). We did not detect GFP-Vas over background levels in unlocalized *nos* and *cycB* particles, but cannot exclude the possibility that there is some Vas associated with these particles.

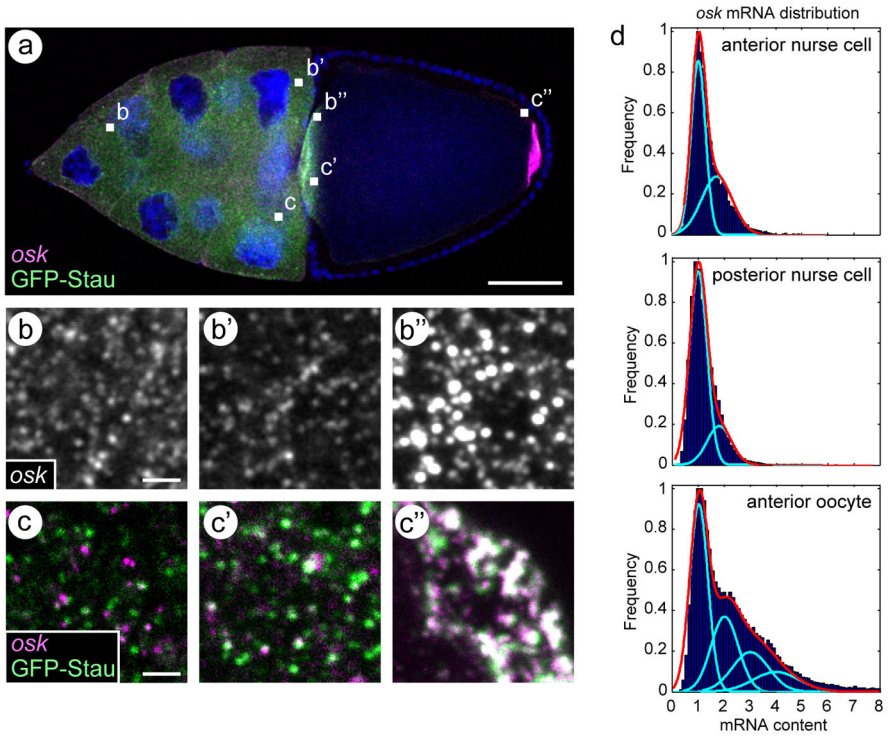

Figure 5. *osk* mRNA forms multimeric complexes upon entry into the oocyte

(a) Low-magnification view of a GFP-Stau stage 10b egg chamber labeled with *osk* probes. Squares indicate regions magnified in (**b-b″**) and (**c-c″**). (**b-b″**) *osk* particles in anterior (**b**) and posterior (**b′**) nurse cells and at the anterior of the oocyte (**b″**). Scale bar: 2 μm. (**c-c″**) *osk* and GFP-Stau in a nurse cell (**c**), at the anterior (**c′**) and at the posterior (**c″**) of the oocyte. Scale bars: 50 μm (**a);** 2 μm (**b**,**c**). (**d)** Histograms of mRNA content for unlocalized *osk* particles in anterior (upper) and posterior (middle) nurse cells, and at the anterior of the oocyte (lower). Cyan lines indicate Gaussian distributions centered on integer numbers of mRNAs. Red lines indicate sums of Gaussians. In anterior nurse cells, fitting to two Gaussians yields 42% of particles containing 2 mRNAs, compared with 22% in posterior nurse cells.

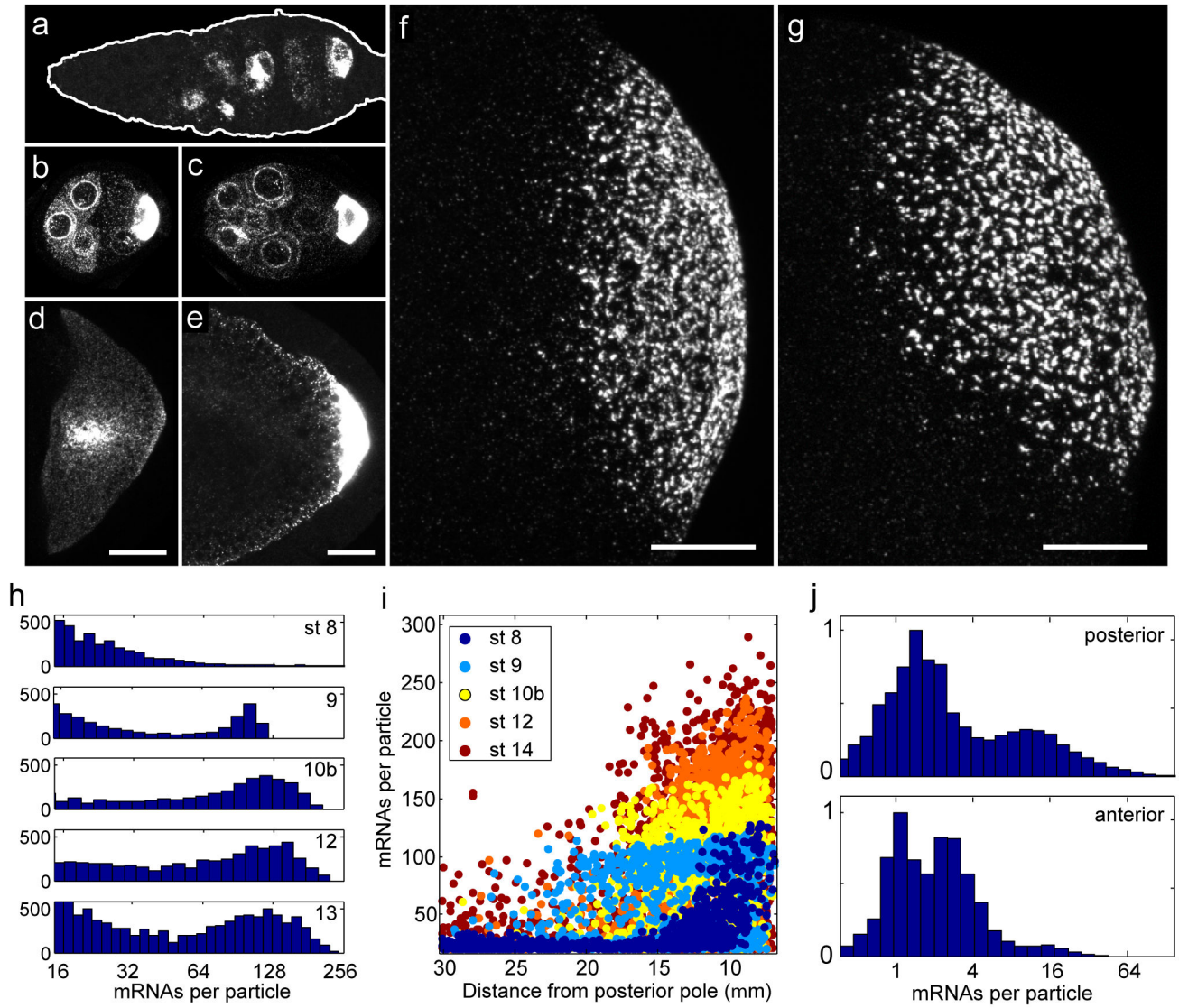

Figure 6. Dynamics of *osk* granule assembly

(a–g) Confocal images showing the distribution of *osk* mRNA throughout oogenesis. Z-series projections are shown in all but (**d**). (**a**) Germarium (outlined) with expression in presumptive nurse cells and accumulation in presumptive oocytes. (**b,c**) Stage 4 (**b**) and stage 6 (**c**) egg chambers displayed at saturating settings to illustrate *osk* expression in nurse cells and high concentration in oocytes. At all stages, anterior nurse cells consistently display higher levels of *osk* than posterior nurse cells. (**d**) Single image plane at stage 7 reveals the transient accumulation of *osk* in the center of the oocyte. (**e**) Stage 10a with strong *osk* enrichment at posterior pole in midsagittal cross-section. (**f,g**) Cortical views at stage 12 (**f**) and stage 14 (**g**). Scale bars: 10 μm (**d,e**); 20 μm (**f,g**). (**h**) Histograms of cortical *osk* particle intensities during mid to late oogenesis. (**i**) *osk* content as a function of distance from posterior pole. (**j**) Normalized distribution of mRNA content of all particles found in confocal z-stacks encompassing the posterior 20% of a stage 13 oocyte (top) and a similarly

sized volume in the center of the oocyte (bottom) illustrating a reduction in the fraction of particles containing 2–4 mRNAs in the posterior domain.

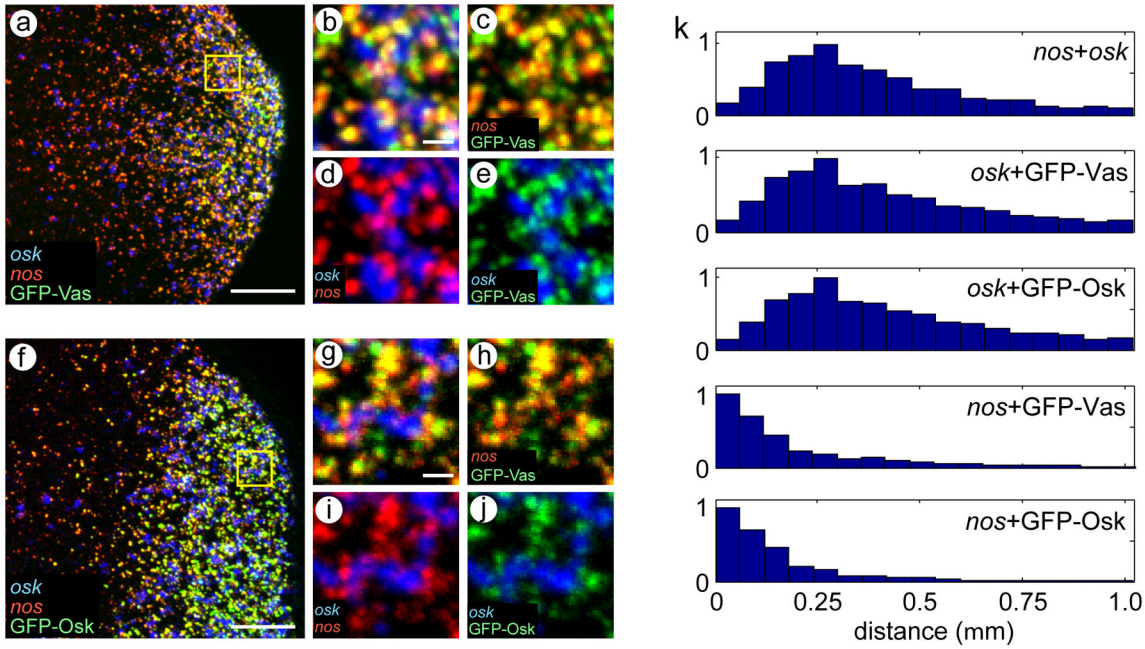

Figure 7. *osk* mRNA is continuously segregated from germ plasm components

(a–e) Maximum z-series projection spanning 5 μm at the posterior cortex of a stage 13 GFP-Vas oocyte and labeled with *osk* and *nos* probes. **(f–j)** Cortical image of a stage 13 Osk-GFP oocyte. (**b–e**, **g-j**) High magnification of boxed regions, showing *osk* mRNA occupying regions devoid of germ plasm components. Scale bars: 10 μm (**a,f**); 1 μm (**b–e**, **g-j**). (**k**) Distribution of distances between nearest neighbors for each pair of particles. Median distance between *osk* and *nos*, GFP-Vas or Osk-GFP is 400 nm, compared to 75 nm for *nos* and either GFP-Vas or Osk-GFP.

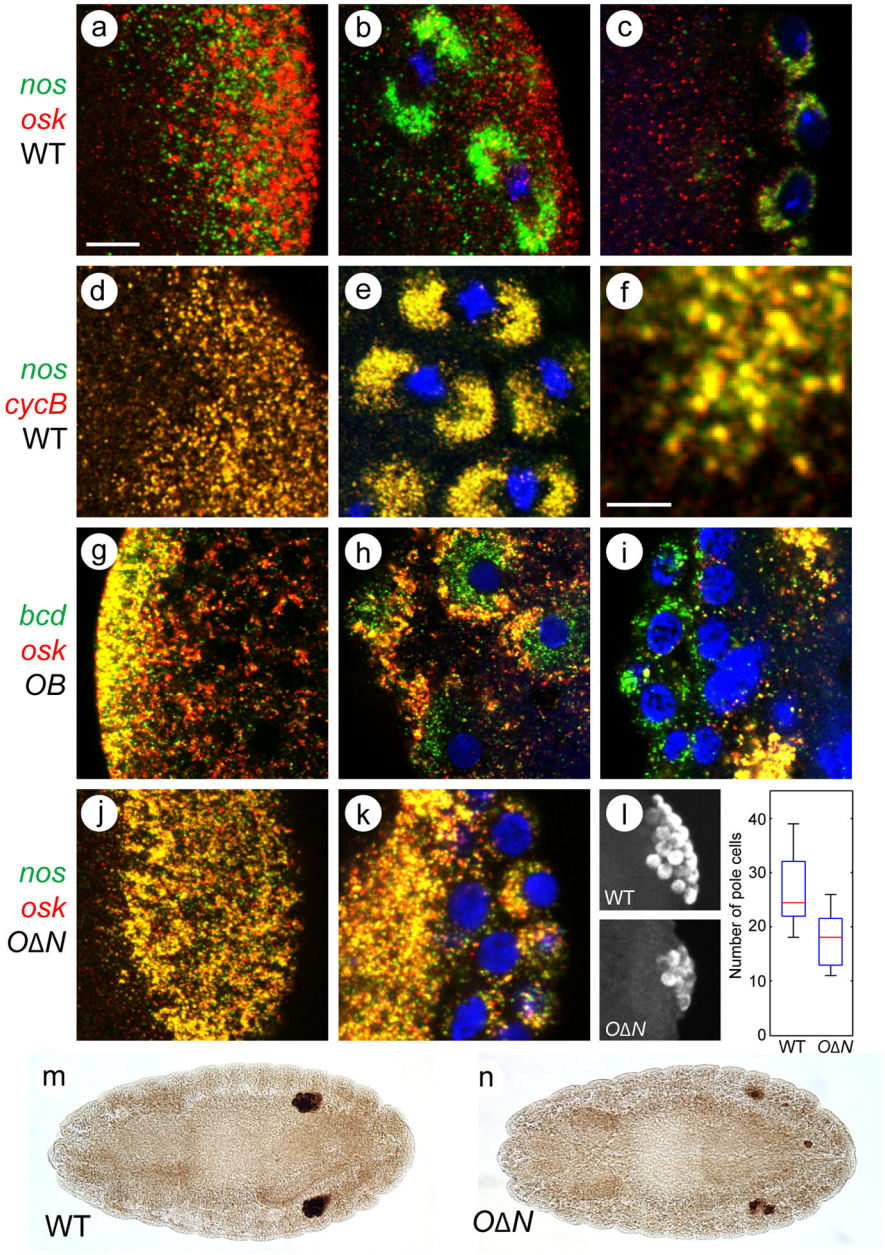

Figure 8. *osk* localization to germ plasm impairs germline development

(a) Confocal section at the cortex of an early (n.c. 2) wild-type (WT) embryo labeled with *nos* and *osk* probes, showing the continued segregation of *nos* and *osk*. (**b)** Enrichment of *nos* on astral microtubules and depletion of large *osk* granules in a n.c. 9 embryo. (**c)** *nos* is highly enriched in pole cells of a blastoderm (n.c. 14) embryo, whereas *osk* is largely absent. *nos* displayed at lower contrast, and *osk* at high contrast, compared to (**a)** and (**b)**. (**d,e)** Co-localization of *nos* and *cycB* during n.c. 3 (**d**) and n.c. 11 (**e**). (**f)** High magnification view of *nos* and *cycB* granules. (**g–i)** FISH analysis of *osk-bcd3′UTR* (*OB*) embryos with *bcd* and *osk* probes. (**g**) Z-series projection of the anterior cortex show co-localization of *bcd* and *osk-bcd3′UTR* mRNAs in granules at n.c. 3. (**h**) Granules containing *osk* are excluded from

the vicinity of presumptive ectopic pole cells at n.c. 10. (**i**) *bcd* particles are enriched in ectopic pole cells at n.c.14, which are largely devoid of *osk*. Most *osk* granules are confined to a region basal to the blastoderm layer. (**j,k)** FISH analysis of *oskΔi1,2-nos3′UTR* embryos (*OΔN*) with *osk* and *nos* probes. Z-series projections of the posterior cortex at n.c. 4 (**j**) and n.c. 14 (**k**) show co-localization of *oskΔi1,2-nos3′UTR* and *nos* through pole cell formation. Scale bars: 10 μm (**a–e**, **g-k**); 2 μm **(f)**. (**l)** Left: Anti-Vas immunofluorescence in wild-type (upper) and *oskΔi1,2-nos3′UTR* (lower) embryos. Right: box plot showing mean (red line), 25th and 75th quartiles (blue boxes), and range (black lines) of Vas-positive pole cell numbers (n=40 wild-type and 59 *oskΔi1,2-nos3′UTR* embryos). **(m,n)** Anti-Vas immunostaining reveals a reduction in Vas-positive cells in the gonads of late-stage *oskΔi1,2-nos3′UTR* embryos.